This article was downloaded by:[Wang, L.-P.]
On: 24 July 2008
Access Details: [subscription number 795306036]
Publisher: Taylor & Francis
Informa Ltd Registered in England and Wales Registered Number: 1072954
Registered office: Mortimer House, 37-41 Mortimer Street, London W1T 3JH, UK

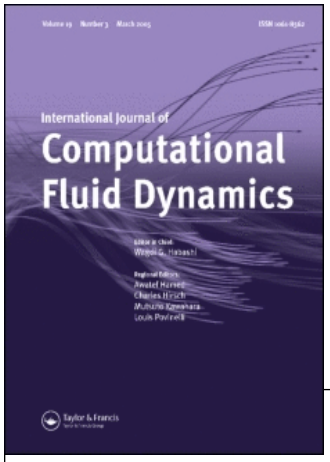

International Journal of Computational Fluid Dynamics
Publication details, including instructions for authors and subscription information:
http://www.informaworld.com/smpp/title~content=t713455064

Modelling microscale flow and colloid transport in saturated porous media

Hui Gao [a]; Jie Han [b]; Yan Jin [b]; Lian-Ping Wang [a]
[a] Department of Mechanical Engineering, University of Delaware, Newark, DE, USA
[b] Department of Plant and Soil Sciences, University of Delaware, Newark, DE, USA

Online Publication Date: 01 August 2008

To cite this Article: Gao, Hui, Han, Jie, Jin, Yan and Wang, Lian-Ping (2008) 'Modelling microscale flow and colloid transport in saturated porous media', International Journal of Computational Fluid Dynamics, 22:7, 493 — 505

To link to this article: DOI: 10.1080/10618560802238259
URL: http://dx.doi.org/10.1080/10618560802238259

PLEASE SCROLL DOWN FOR ARTICLE

Full terms and conditions of use: http://www.informaworld.com/terms-and-conditions-of-access.pdf

This article maybe used for research, teaching and private study purposes. Any substantial or systematic reproduction, re-distribution, re-selling, loan or sub-licensing, systematic supply or distribution in any form to anyone is expressly forbidden.

The publisher does not give any warranty express or implied or make any representation that the contents will be complete or accurate or up to date. The accuracy of any instructions, formulae and drug doses should be independently verified with primary sources. The publisher shall not be liable for any loss, actions, claims, proceedings, demand or costs or damages whatsoever or howsoever caused arising directly or indirectly in connection with or arising out of the use of this material.

International Journal of Computational Fluid Dynamics
Vol. 22, No. 7, August 2008, 493–505

Taylor & Francis
Taylor & Francis Group

Downloaded By: [Wang, L.-P.] At: 20:54 24 July 2008

Modelling microscale flow and colloid transport in saturated porous media

Hui Gao[a], Jie Han[b], Yan Jin[b] and Lian-Ping Wang[a]*

[a]*Department of Mechanical Engineering, University of Delaware, Newark, DE, USA;* [b]*Department of Plant and Soil Sciences, University of Delaware, Newark, DE, USA*

(*Received 7 May 2008; final version received 29 May 2008*)

The microscale flow in soil porous media determines the transport of colloids contained in groundwater. In this paper, two completely different computational approaches, namely a mesoscopic lattice Boltzmann approach and a Navier–Stokes based hybrid approach, are applied to simulate pore-scale viscous flows. The porous medium is represented by a channel partially filled with circular (in 2D) or spherical (in 3D) particles. We demonstrate that the two approaches produce almost identical pore-scale flow field, providing a rigorous cross-validation for each approach. A Lagrangian particle-tracking approach is then used to study the transport of colloids in these flows. Due to the competing effects of hydrodynamic forces and electro-chemical interactions, it is shown that enhanced removal of colloids from the fluid by solid surfaces occurs when the residence time of colloids in a given flow passage is increased, in qualitative agreement with pore-scale visualisation experiments using confocal microscopy.

Keywords: porous medium; saturated soil; pore-scale flow; direct numerical simulation; lattice Boltzmann method; colloid retention

1. Introduction

Understanding the mechanisms of colloid retention and transport in soil porous media is of importance to the management of groundwater contamination by contaminants that could sorb to and migrate with mobile colloids or by pathogenic microorganisms. Even for the relatively simple case of saturated soil and aquifer, the transport of colloids and their attachment to solid surfaces are governed by a multitude of physical processes: transport by low-speed microscale water flows, Brownian motion due to random thermal fluctuation and a variety of electro-chemical interactions between colloids and solid surfaces (Elimelech *et al.* 1995, Chu *et al.* 2000). These physical processes together encompass a large range of length scales from millimetre scale to nanometre scale, with each possibly dominating the motion of a colloid depending on the colloid's relative location within a pore-scale passage. A quantitative modelling tool requires both an accurate pore-scale flow simulation and a realistic representation of all important colloid–surface interaction forces.

This paper concerns mainly the accurate simulation of complex flows at the pore-scale. This will be addressed by employing two completely different computational approaches to a given flow problem. First, we will explore the use of lattice Boltzmann method (LBM) as a simulation tool for viscous flow through a porous medium. The LBM approach is based on a kinetic formulation and has certain advantages over the traditional Navier–Stokes based computational fluid dynamics (Qian *et al.* 1992, Chen and Doolen 1998). While LBM models capable of addressing thermal flows, flows through porous media, multiphase flows, electro-osmotic flows and contact line, etc. have been proposed in recent years, two general aspects remain to be studied before they can be applied to complex flow modelling. The first aspect concerns the accuracy and reliability of these LBM models for practical applications. Since these models have typically only been tested for idealised problems, their applications to complex flow problems need to be critically examined and different possible LB models are compared. The second aspect concerns a variety of LBM implementation issues when dealing with practical applications.

Since accurate local measurements of pore-scale microscale flows are not usually feasible, our strategy here is to introduce a second, Navier–Stokes based computational approach. The hybrid approach, referred to as Physalis by its original developers (Takagi *et al.* 2003), integrates a numerical solution of discretised Navier–Stokes equation on a simple uniform grid with an analytical representation of local flow near the surface of a solid particle. Direct comparisons between LBM and Physalis offer an opportunity for cross-validating each approach as well as contrasting their pros and cons.

As the first step, we focus our attention on a 2D model of porous media, namely, a 2D channel partially filled with fixed circular cylinders. After the accuracy of the flow

*Corresponding author. Email: lwang@udel.edu

ISSN 1061-8562 print/ISSN 1029-0257 online
© 2008 Taylor & Francis
DOI: 10.1080/10618560802238259
http://www.informaworld.com

Downloaded By: [Wang, L.-P.] At: 20:54 24 July 2008

simulation is established, the trajectories of colloids are simulated under the influence of Stokes drag, Brownian force and electro-chemical surface–interaction forces. The rate of deposition of colloids on solid surfaces at a given solution ionic strength is then analysed for several flow speeds. A thorough analysis of colloid deposition under various conditions can be found in our companion paper (Han *et al.* 2008).

2. Methodology

Consider a viscous flow in a 2D channel with seven fixed cylinders as shown in Figure 1. This 2D setting is used to mimic a slice of a 0.8 mm × 0.8 mm channel packed with glass beads (0.20 mm in diameter, i.e. Figure 10 below). Flow is driven by a constant pressure gradient or a body force in the y-direction. Periodic boundary condition is assumed in flow direction with a periodicity length of L, while no-slip velocity condition is applied on the two sidewalls at $x = 0$ and H, and on the surface of the seven glass cylinders. The channel width H is set to 200 and the cylinders have an identical diameter of 30. The computational domain size in terms of the grid spacing ($dx = dy = 1$) is 200 in the x-direction and 93 in the y-direction. The centres of the seven cylinders are located at (50,25), (100,25), (150,25), (25,68), (75,68), (125,68) and (175,68), respectively.

At the initial time $t = 0$, the fluid is at rest. The body force per unit volume is set to $F_B = 8\rho\nu U_c/H^2$, such that the centreline velocity of the channel would be U_c at long time when the body force is balanced by the viscous effects, if there were no glass cylinders in the channel. Here, ν and ρ are the fluid kinematic viscosity and density, respectively. The magnitude of U_c is adjusted to match the flow rate in our microchannel flow experiment. For the results discussed here, U_c is such that the Reynolds number based on U_c and H is $U_cH/\nu = 0.20025$.

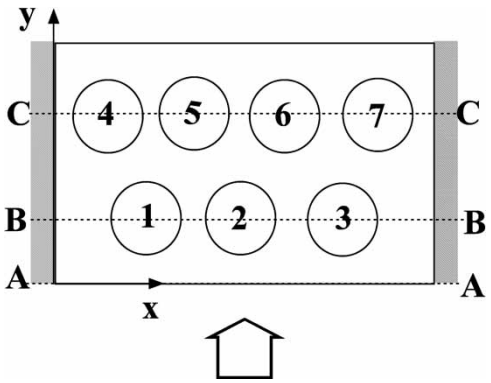

Figure 1. A sketch of the 2D channel with seven fixed glass beads.

2.1 The lattice Boltzmann approach

In the LBM approach, the lattice Boltzmann equation for the distribution function f_i of the mesoscopic particle with velocity $\mathbf{e}_i$:

$$f_i(\mathbf{x} + \mathbf{e}_i\delta_t, t + \delta_t) - f_i(\mathbf{x}, t) = -\frac{1}{\tau}\left[f_i(\mathbf{x}, t) - f_i^{(\mathrm{eq})}(\mathbf{x}, t)\right] + \psi_i(\mathbf{x}, t), \quad (1)$$

is solved with a prescribed forcing field ψ_i designed to model the driving pressure gradient or body force. In this work, ψ_i is specified as $\psi_i(\mathbf{x}, t) = W_i\mathbf{e}_i\cdot\mathbf{F}/c_s^2$, where $\mathbf{F}$ is the macroscopic force per unit mass acting on the fluid. The standard D2Q9 lattice model in 2D and the D3Q19 model in 3D (Qian *et al.* 1992) are used with the following equilibrium distribution function:

$$f_i^{(\mathrm{eq})}(\mathbf{x}, t) = W_i\left[\rho + \frac{\rho_0\mathbf{e}_i\cdot\mathbf{u}}{c_s^2} + \frac{\rho_0\mathbf{u}\mathbf{u} : \left(\mathbf{e}_i\mathbf{e}_i - c_s^2\mathbf{I}\right)}{2c_s^4}\right], \quad (2)$$

where W_i is the weight, the sound speed c_s is $1/\sqrt{3}$ and $\mathbf{I} \equiv [\delta_{ij}]$ is the second-order identity tensor. The mean density ρ_0 is set to 1. The macroscopic hydrodynamic variables are computed as:

$$\rho = \sum_i f_i, \quad \rho_0\mathbf{u} = \sum_i f_i\mathbf{e}_i, \quad p = \rho c_s^2, \quad (3)$$

where ρ, $\mathbf{u}$ and p are the fluid density fluctuation (the local fluid density is $\rho_0 + \rho$), velocity and pressure, respectively. The above form of the equilibrium distribution was suggested by He and Luo (1997) to best model the incompressible Navier–Stokes equation.

A uniform lattice is used to cover the computational domain. The straight channel walls are located in the middle of lattice links so a second-order accuracy is achieved with a simple bounce-back implementation. The inlet and outlet are also located half way on the lattice links to facilitate the implementation of the periodic boundary condition in the y-direction.

The key implementation issue here is the treatment of solid particle surfaces. For each lattice node near a particle surface, we identify all links moving into the surface and their relative boundary-cutting location, namely, the percentage (α) of a link located outside the surface. Since particles are fixed, this information is pre-processed before the flow evolution. Before the streaming step, the missing population is properly interpolated in terms of α and two populations lying before and after the path of the missing population (Lallemand and Luo 2003, Yu *et al.* 2003). For results in this paper, we used the first-order interpolation based on two known populations and found that the results are quite similar to the second-order interpolation based on three nodes (Lallemand and Luo 2003). All lattice nodes lying within the solid particles

Downloaded By: [Wang, L.-P.] At: 20:54 24 July 2008

(including the fluid–solid interface) are excluded from lattice Boltzmann equation (LBE) evolution, their velocities are simply set to zero. As a validation check, the total mass for the fluid nodes (excluding the fluid–solid interface nodes) is computed and found to remain constant as time is advanced.

We also tested the generalised LBE or the multiple-relaxation-time (MRT) model as presented in Lallemand and Luo (2000) and d'Humières *et al.* (2002). The MRT has been shown to improve numerical stability so flows at higher Reynolds numbers can be simulated. Here, our flow is at low flow Reynolds number, but we will demonstrate an interesting robustness of MRT which allows a wider range of relaxation parameter (or viscosity setting) to be used in the LBM approach, when compared to the usual Bhatnagar–Gross–Krook (BGK) collision model shown in Equation (1).

2.2 *The Navier–Stokes approach: physalis*

To validate the lattice Boltzmann approach and compare it with traditional Navier–Stokes based computational approaches, we also developed a code using the hybrid method proposed by Takagi *et al.* (2003) and Zhang and Prosperetti (2003, 2005). The method was named *Physalis* (Takagi *et al.* 2003). Physalis combines a numerical discrete representation of the Navier–Stokes viscous flow around particles and an analytical representation imbedded near the surface of each particle.

The basic idea behind Physalis is as follows. Because of the no-slip boundary conditions on its surface, a solid particle induces a specific local flow structure that could be used to linearise the Navier–Stokes equations in the neighbourhood of the particle surface. The fluid velocity, pressure and vorticity near the particle surface can be expressed analytically using series solutions of Stokes flow equations. As a result, the geometric surface of the particle can be replaced by a Stokes flow solution valid in a narrow but finite region near the surface, known as the cage region as indicated by the two dash circles in Figure 2.

There are three main components in Physalis. The first component is an analytical representation of the flow within the cage region. This is obtained by the method of separation of variables applied to Stokes flow equations. The general form in 2D is given in Zhang and Prosperetti (2003) and in 3D is found in Zhang and Prosperetti (2005) and Gao and Wang (2007). The second component is the numerical method for Navier–Stokes equations on a regular mesh (the flow solver). The second-order projection method (Brown *et al.* 2001) is used. The intermediate velocity in the fractional step procedure is solved by a factorisation method (Kim and Moin 1985), while the Poisson equation for the projection step is solved by a combination of transformation and tridiagonal inversion. This mesh extends to the interior of the particle surface. The velocity cage essentially defines an internal boundary for the viscous flow where the Stokes solution is employed to specify the boundary conditions there.

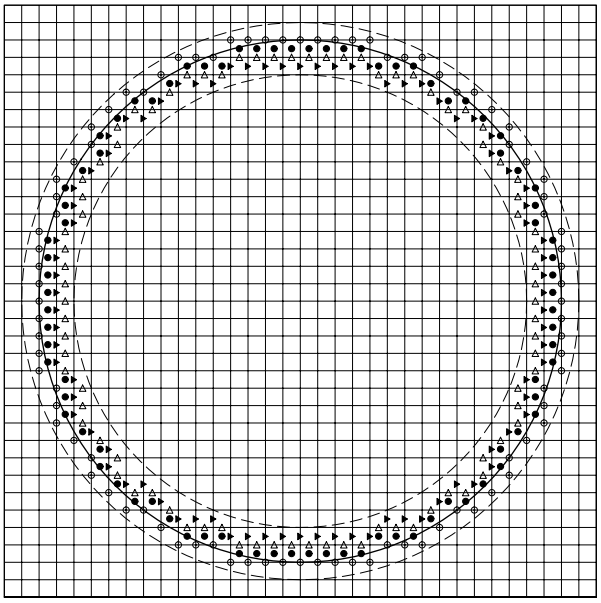

Figure 2. The cage used to represent a glass bead surface in Physalis, for a glass bead with a radius of 15 grid spacings. Solid circles denote pressure cage nodes, open circles are vorticity cage nodes, filled triangles are u-velocity cage nodes and open triangles are v-velocity cage nodes. The thick line denotes the glass bead surface.

The most essential component is the coupling or matching between the numerical solution on the regular mesh and the Stokes solution in the cage. This coupling is achieved by an iterative procedure in which (a) the numerical solution is used to refine the coefficients in the Stokes flow representation and in turn (b) the numerical solution is refined by an updated boundary condition at the velocity cage from the refined Stokes flow. The first part is accomplished by a singular value decomposition algorithm, since an over-specified linear system (the number of cage nodes used for coupling is larger than the number of coefficients) is to be solved. The second part currently relies only on the specific method of defining the cage velocity nodes or the internal boundary, so the analytical nature of the Stokes solution may not be fully taken advantage of. There is more than one way to specify the cage region (Takagi *et al.* 2003). For accuracy of the Stokes flow representation, it is desirable to select the cage nodes as close to the surface of the particle as possible.

An important advantage of this hybrid method is that the force and torque acting on the particle can be calculated directly from the Stokes solution, avoiding often tedious numerical integration of local viscous force on the particle surface that is necessary for other non-hybrid numerical methods.

Downloaded By: [Wang, L.-P.] At: 20:54 24 July 2008

2.3 Dynamics of colloids

When the steady viscous flow is established in the microscale porous channel, colloids are randomly injected into the flow at the inlet with a velocity equal to the local fluid velocity, at a rate that corresponds to a concentration of 1 ppm. One ppm indicates that the colloid mass concentration is 1 mg/l or a number concentration of 1810 per mm^3 of the solution. If we assume that the 2D flow model represents a slice of thickness equal to the colloid radius, then the above concentration implies that there are about 23.7 colloids in the periodic fluid domain shown in Figure 1.

Since this concentration is very low, the fluid flow is assumed to be unaffected by the presence of colloids. Each colloid is treated as a discrete entity (point-like particle) and moves according to the following equation of motion:

$$m_c \frac{d\mathbf{v}(t)}{dt} = \mathbf{F}^{drag} + \mathbf{F}^b + \mathbf{F}^g + \mathbf{F}^B + \mathbf{F}^c, \qquad (4)$$

where $\mathbf{v}(t)$ is the instantaneous (Lagrangian) velocity of the colloid, $m_c \equiv 4\pi\rho_c a_c^3/3$ is the mass of the colloid, ρ_c is the material density of the colloid and a_c is the radius of the colloid. All relevant physical parameters and their corresponding value in the numerical simulation are shown in Table 1. The hydrodynamic forces include the viscous drag $\mathbf{F}^{drag}$ and the buoyancy force $\mathbf{F}^b$. Other forces such as the pressure-gradient force, the added mass and Basset history term (Maxey and Riley 1983) are neglected here due to the very slow solvent (water) flow. $\mathbf{F}^g$ is the gravitational body force. $\mathbf{F}^B$ is a random force designed to simulate Brownian motion of the colloid due to local thermal fluctuations of solvent molecules. Finally, $\mathbf{F}^c$ represents interaction forces of the colloid with the glass (grain and wall) surface or other deposited colloids. The colloid is assumed to have a radius of $a_c = 0.5\,\mu m$, this together with the slow Stokes flow of the solvent implies that a Stokes drag could be assumed, namely:

$$\mathbf{F}^{drag} = \zeta(\mathbf{u}(\mathbf{Y}(t), t) - \mathbf{v}(t)), \quad \text{with } \zeta \equiv 6\,\pi\mu a_c, \qquad (5)$$

where $\mathbf{u}(\mathbf{x},t)$ is the Eulerian solvent velocity field, $\mathbf{Y}(t)$ is the instantaneous location of the colloid obtained from the kinematic equation $d\mathbf{Y}(t)/dt = \mathbf{v}(t)$ and μ is the solvent viscosity. As the first step, we neglected the effects of local fluid shear and any corrections of the viscous force due to glass cylinder surface or channel wall. Local shear flow may induce viscous force (i.e. lift force) normal to the flow (Saffman 1965, McLaughlin 1991). Hydrodynamic interaction of the colloid with a surface can result in a modified drag, additional lift and non-zero torque (Goldman *et al.* 1967, O'Neill 1968). These modifications could be included in our Lagrangian colloid-tracking approach. Here, we chose to keep the force formulation simple for the following reasons: (a) in a study conducted by Arcen *et al.* (2006), it was shown that the results of particle statistical properties from numerical simulation based on the standard drag force only are not much different from these obtained using wall-corrected drag and lift forces; (b) computations of wall and shear corrections are computationally expensive; (c) there appear to be inconsistencies in the literature regarding the general expression of viscous force acting on a particle in a shear flow near a surface and (d) we intend to develop a systematic understanding by gradually adding complexity to the description of hydrodynamic forces, one step at a time.

The Stokes inertial response time of the colloid $\tau_c \equiv m_c/\zeta = 2\rho_c a_c^2/(9\mu)$ is about 5.86×10^{-8} s, which is much smaller than the typical flow time scale. Therefore, the colloid would move along a streamline if no other

Table 1. Physical parameters and their values in the numerical simulation.

	Symbol	Physical value	Value in simulation
Water density	ρ	1000 kg/m^3	1
Water viscosity	μ	0.001 kg/(m·s)	0.8
Grid spacing	dx, dy	2 μm	1
Channel width	H	800 μm	400
Periodicity length	L	372 μm	186
Glass cylinder radius	R	60 μm	30
Colloid radius	a_c	0.5 μm	0.25
Velocity used in setting F_B	U_c	679.5 m/day	0.01258
Mean speed realised	U_s	2.887 m/day	5.347×10^{-5}
Porosity	ϵ	0.734	0.734
Nominal flow speed	U_s/ϵ	~ 4.0 m/day	7.285×10^{-5}
Colloid density	ρ_c	1055 kg/m^3	1.055
Time step	dt	6.4×10^{-5} s	20
Mass of colloid (actual)	m_c	5.524×10^{-16} kg	0.06905
Mass of colloid (assumed)	m_c^*	6.033×10^{-12} kg	754.0
Response time (actual)	τ_c	5.86×10^{-8} s	1.831×10^{-2}
Response time (assumed)	τ_c^*	6.4×10^{-4} s	200
Force	$\mathbf{F}^{drag}$, $\mathbf{F}^c$, etc.	$(1.563 \times 10^{-9})\mathbf{F}$ N	$\mathbf{F}$

Downloaded By: [Wang, L.-P.] At: 20:54 24 July 2008

forces were considered. In the numerical simulation, we assumed a value of $\tau_c^* = 6.4 \times 10^{-4}$ s, which is several orders of magnitude larger than the actual value, but is still very much smaller than the flow time scale, in order to reduce the stiffness of the system, Equation (4), so a large integration time step can be used. Note that the typical flow time scale is on the order of $a_c/U_s = 0.5$ s. Numerical tests show that the results are not sensitive to the value of τ_c as long as it is much smaller than the typical flow timescale.

The buoyancy force and body force together is given as:

$$\mathbf{F}^{bg} = \mathbf{F}^{b} + \mathbf{F}^{g} = m_c\left(1 - \frac{\rho_w}{\rho_c}\right)\mathbf{g}, \tag{6}$$

where ρ_w is the solvent density and $\mathbf{g}$ is the gravitational acceleration. Taking the density ratio of $\rho_c/\rho_w \approx 1.055$ and $|\mathbf{g}| = 9.8\,\mathrm{m/s^2}$, the ratio of $\mathbf{F}^{bg}$ to $\mathbf{F}^{drag}$ may be estimated as $m_c(0.052)g/(\zeta U_s) = 0.052\tau_c/(U_s/g) \approx 0.894 \times 10^{-3}$ (see Table 1). Furthermore, the 2D simulation considered here is viewed as modelling the transport of colloids in a horizontal plane section through the actual 3D horizontal porous channel. For these reasons, here, we neglected the buoyancy force and body force together.

The Brownian force is specified as $\mathbf{F}^B = (F_1^B, F_2^B)$, where each component F_i^B is an independent Gaussian random variable of zero mean and the following standard deviation (Fujita *et al.* 2004):

$$\sigma_{F_i^B} = \sqrt{\frac{2\zeta kT}{\mathrm{d}t}}, \tag{7}$$

where dt is the time step size, T is the temperature (assumed to be 293 K), $k = 1.38 \times 10^{-23}$ J/K is the Boltzmann constant. When a simple explicit Euler scheme is applied, the Brownian force would generate the desired mean square value (kT/m_c) of velocity fluctuation in each direction (Elimelech *et al.* 1995). The ratio of the Brownian force to the drag force is estimated to be $\sqrt{2\tau_c kT/\left(m_c U_s^2 \mathrm{d}t\right)} \approx 3.5$, implying that the Brownian effect is as important as the drag force in transporting the colloidal particles. The above treatment for the Brownian motion is based on a stochastic (Langevin equation) model. It should be noted that an alternative would be to directly introduce fluctuating hydrodynamics (Landau and Lifshitz 1959) within the LBE, as performed in Ladd (1993).

While the drag force and the Brownian force are active in all regions of the flow domain, the colloidal interaction force is a short-range force that is only important when a colloid is very close to a glass surface or another deposited colloid. It consists of the electrostatic, Lifshitz–van der Waals (LW) and Lewis acid–base (AB) interaction forces (van Oss 1994):

$$F^c = F^{EDL} + F^{LW} + F^{AB}, \tag{8}$$

where all interaction forces are assumed to act in the direction normal to a surface, with a positive value indicating a repulsive force and negative an attractive force. The formulation of these forces is primarily based on the Derjaguin and Landau (1941) and Verwey and Overbeek (1948) (DVLO) interaction potential. The electrostatic double layer (EDL) force results from the interaction of a charged particle with the ions in the liquid medium. For colloid–glass surface interaction, the EDL force may be written as Hogg *et al.* (1966) and Han *et al.* (2008):

$$F^{EDL,\,cg} = \frac{a_c\kappa}{1 - \exp(-2\kappa h)} \times [\alpha_1 \exp(-\kappa h) - \alpha_2 \exp(-2\kappa h)], \tag{9}$$

where h is the minimum gap between the colloid and a glass surface (the distance from the centre of the colloid to the surface minus a_c), κ is the inverse Debye–Huckel screening length, which depends on the solution ionic strength. Here, we shall only consider an ionic strength at 100 mM in NaCl electrolyte solution and in this case $1/\kappa = 0.963$ nm. The coefficients α_1 and α_2 are related to the surface potentials of the glass surface (−69.74 mV) and colloid (−76.99 mV) as well as the dielectric constant of the medium (Han *et al.* 2008). The surface potentials are computed based on the measured ζ-potentials (−41.31 and −45.56 mV, respectively; Han *et al.* 2008). For the electrolyte solution used in this study (Han *et al.* 2008), $\alpha_1 = 4.648 \times 10^{-11}$ N and $\alpha_2 = 4.671 \times 10^{-11}$ N. With the above parameters, the EDL force is repulsive and $F^{EDL}/(\zeta U_s) > 1$ when $h/a_c < 0.02$ (Figure 3). For the case of colloid–colloid interaction at 100 mM ionic strength, the EDL force is computed by Elimelech *et al.* (1995) and Han *et al.* (2008):

$$F^{EDL,\,cc} = (1.847 \times 10^{-11}\,\mathrm{N})a_c\kappa \exp(-\kappa h), \tag{10}$$

where h is the minimum gap between the two approaching colloids.

The attractive LW interaction accounts for intermolecular interaction including London dispersion, Keesom dipole–dipole and Debye induction. For the purpose of this paper, the LW force can be written as van Oss (1994) and Han *et al.* (2008):

$$F^{LW,\,cg} = -\beta a_c\left(\frac{h_0}{h}\right)^2, \tag{11}$$

where h_0 is an equilibrium distance used to model the occurrence of physical contact and is set to 0.157 nm (Elimelech *et al.* 1995). The constant β has been determined to be 0.0434 J/m^2 for colloid–surface interaction and 0.0469 J/m^2 for colloid–colloid interaction, based on the

Downloaded By: [Wang, L.-P.] At: 20:54 24 July 2008

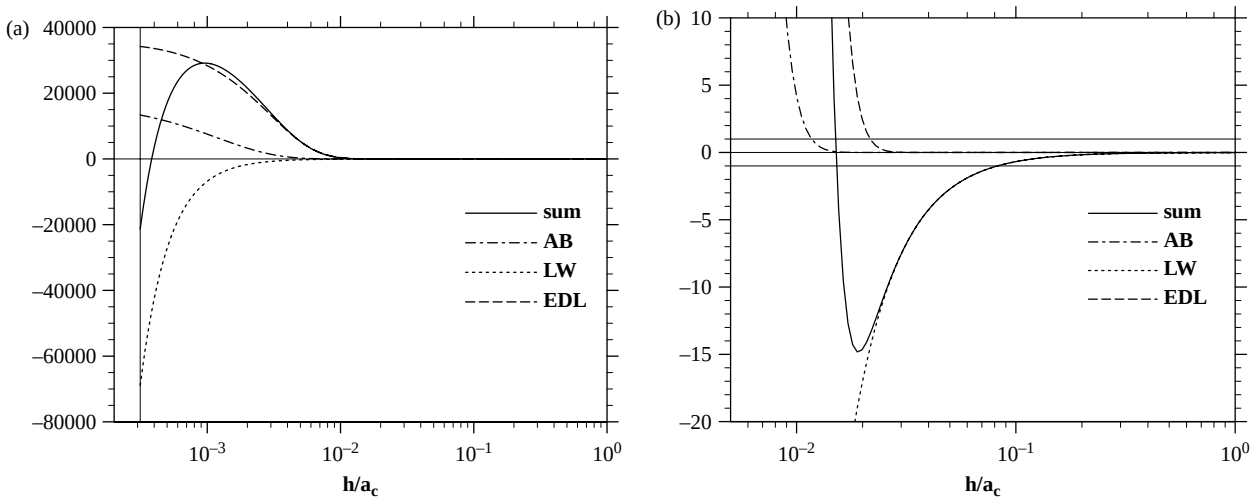

Figure 3. Different colloidal interaction forces normalised by (ζU_s) for colloid–surface interaction: (a) the region $h_0 < h < a_c$ and (b) the zoom-in region $0.005a_c < h < a_c$. The thin vertical line in (a) marks the location where $h = h_0$. The three horizontal lines in (b) mark the value of -1, 0 and 1, respectively.

thermodynamic parameters of colloids, glass and the liquid solution.

The AB force originates from the bonding reaction of a Lewis acid and a Lewis base. It can be expressed as van Oss (1994) and Han *et al.* (2008):

$$F^{\mathrm{AB}} = -\gamma \frac{h_0 a_c}{\chi} \exp\left(\frac{h_0 - h}{\chi}\right), \tag{12}$$

where $\chi = 0.6$ nm is the water decay length (van Oss 1994), the constant γ is determined, using the relevant electron-accepter and electron-donor parameters, to be -0.0322 and $-0.170\,\mathrm{J/m^2}$ for colloid–surface and colloid–colloid interactions, respectively.

In Figure 3, we compare the three different colloidal interactions forces and also their magnitudes relative to the drag force, for the case of colloid–glass surface interaction. Several important observations can be made. First, as a colloid approaches a surface, the LW attractive force is the first active force and it plays a role starting at $h \approx 0.2\,a_c$. This attractive LW force dominates the colloidal interaction until $h \approx 0.02\,a_c$, with a peak magnitude at least 10 times the drag force. Then the EDL force quickly takes over to turn the net interaction force a repulsive force. An important parameter here is $\kappa a_c = 519.2$, implying that the EDL force will play a role when the gap is on the order of $a_c/519.2 = 0.00193\,a_c$. This scale indeed falls in the range when EDL force is the dominant force. Eventually at $h/a_c \approx 0.0004$, the LW force wins over to change the net force back to an attractive force (i.e. towards the primary energy minimum). This overall picture implies that the LW force is the dominant force acting over most of the small gap distances. The two locations where the net force is zero, namely, $h/a_c = 0.000383$ and 0.0152, correspond to the secondary minimum and the energy barrier in the net energy potential (Elimelech *et al.* 1995).

Similar plots are shown in Figure 4 for the interaction of a colloid with another deposited colloid. In this case, the net interaction force at $h = h_0$ is repulsive, implying the surface location where a colloid has been deposited will not attract a second colloid. The net force variation near the secondary minimum is similar.

In our simulation, both the grain and wall surface are treated as a flat glass surface. For a given colloid particle, all possible colloid–surface and colloid–colloid binary pair interactions are summed to obtain the final $\mathbf{F}^c$. Such pairwise summation of all the binary interactions is a reasonable approach since here, $\kappa a_c >> 1$ (Das and Bhattacharjee 2005). The equation of motion was solved numerically by first integrating the drag force and colloidal force using a mixed fourth-order Adam–Bashforth and Adman–Moulton scheme. The Brownian force was then added using the explicit Euler scheme.

3. Results

3.1 Viscous flow simulation

Before discussing the results for the flow problem shown in Figure 1, we shall validate both our LBM and Physalis codes by a unit cell flow problem in which a fixed cylinder of radius a is located at the centre of a 2D channel with walls at $x = 0$ and H. Periodic flow condition is assumed in the y-direction with periodicity length of L. Both channel walls are moving at a constant velocity of U. The force F_y acting on the cylinder in the flow direction is of interest. This simulates a problem of viscous flow over a line of cylinders with spacing equal to L, driven by two moving walls both

Downloaded By: [Wang, L.-P.] At: 20:54 24 July 2008

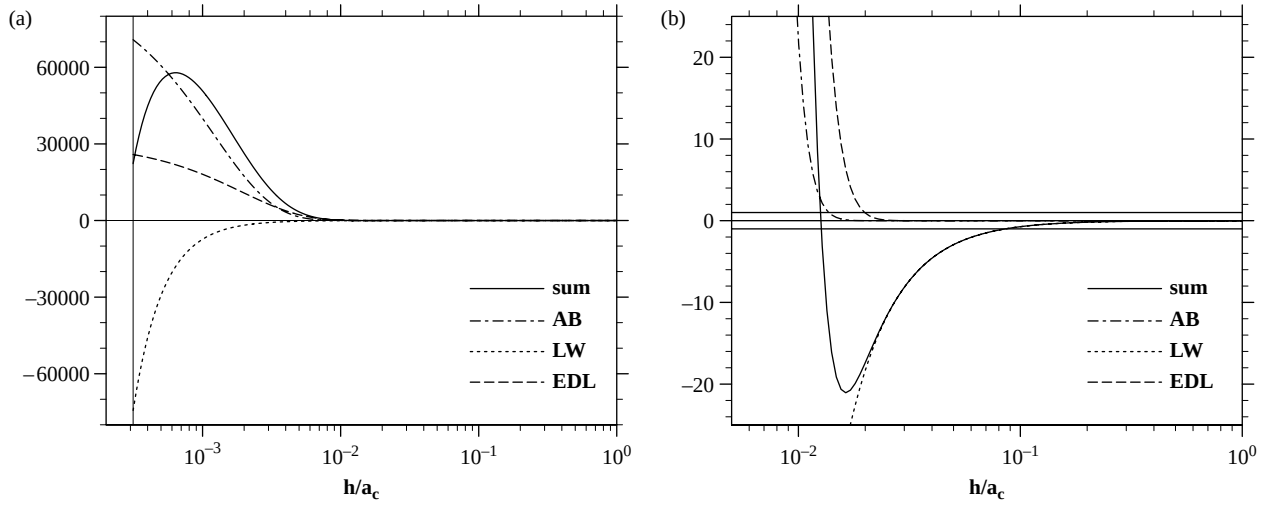

Figure 4. Different colloidal interaction forces normalised by (ζU_s) for colloid–colloid interaction: (a) the region $h_0 < h < a_c$ and (b) the zoom-in region $0.005a_c < h < a_c$. The thin vertical line in (a) marks the location where $h = h_0$. The three horizontal lines in (b) mark the value of -1, 0 and 1, respectively.

parallel to the line and located $H/2$ away from the line. Clearly, the normalised force $F_y/(2\pi\rho U^2 a)$ is a function of three dimensionless parameters: the Reynolds number $Re = \rho U(2a)/\mu$ and the two geometric scale ratios $L/(2a)$ and L/H, where ρ and μ are fluid density and viscosity. Here, we set $Re = 1$ and $L/H = 1$. The resulting normalised forces are shown in Table 2 for three different $L/(2a)$ ratios. In our simulations, the unit cell is discretised at a mesh resolution of 144 × 144, 64 × 64 and 24 × 24 for cases A–C, respectively, which corresponds to a very moderate resolution of the cylinder radius at $a/\delta x = 6.102$, 5.246 and 5.742, for the three cases, respectively. The density and the mesh spacing are assumed to be one for all runs. For the LBM simulations, the relaxation time is set to $\tau = 1$ so the kinematic viscosity is $\mu/\rho = 1/6$. For Physalis, the wall velocity U is set to 0.1. Only the force at the steady state is presented here. Table 2 shows that our LBM and Physalis results are always within 1% to each other. Our results are also in very good agreement with the previous results of Inamuro *et al.* (2000) and Zhang and Prosperetti (2003).

We now consider the flow problem shown in Figure 1. Both LBM and Physalis codes were developed to simulate this flow. The steady-state mean flow speed U_s, defined as the volumetric flow rate per unit depth normalised by H, is much smaller than U_c and is found to be 0.00425 U_c. Therefore, the flow Reynolds number based on the mean speed is $U_s H/\nu = 8.51 \times 10^{-4}$ or the flow in the microchannel is essentially a Stokes flow. It is then expected that the flux is linearly related to the applied forcing.

Figure 5 compares the resulting flow volumetric flux normalised by $0.01\,HU_c$. The parameters used in Physalis are $U_c = 8.01 \times 10^{-4}$, $\rho = 1$, $\nu = 0.8$ and the time step size $dt = 10$, while in the LBM simulation, $U_c = 4.171875 \times 10^{-5}, \rho = 1, \nu = 0.0416667$ (or $\tau = 5/8$) and $dt = 1$. These settings imply that one Physalis time step corresponds to roughly 192 LBM time steps, although, we can adjust the LBM parameters to improve the efficiency of the LBM simulation (see below). During the transient development, the flux increases monotonically with time, reaching to its steady-state value at a non-dimensional time of about $tU_c/H = 0.001$. The steady state value for LBM is only 1% different from the Physalis result. This comparison between LBM and Physalis is obtained when the truncation order for the local Stokes flow representation in Physalis is set to 6 (or a total of 26 expansion coefficients are considered, Zhang and Prosperetti (2003) for detail). It was also found that even with a low truncation order of two in Physalis (i.e. 10 expansion coefficients), the steady-state flux is only 2% different from the IBM result. This shows that, on the one hand, the local flow structure near the cylinder surface is relatively smooth, but at the same time, the interaction between the cylinders and with the channel walls induces secondary higher-order corrections. The Stokes flow truncation order at six will be assumed for all the comparisons below.

Table 2. Comparison of the normalised force acting on a fixed cylinder in a unit cell flow driven by two moving walls.

Case	$L/(2a)$	LBM	Physalis	ZP03[a]	IMO00[b]	AL95[c]
A	11.8	1.033	1.033	1.034	1.053	0.966
B	6.1	1.241	1.243	1.224	1.251	1.158
C	2.09	2.098	2.083	2.079	2.093	2.067

[a] Zhang and Prosperetti (2003).
[b] Inamuro *et al.* (2000).
[c] Aidun and Lu (1995).

Downloaded By: [Wang, L.-P.] At: 20:54 24 July 2008

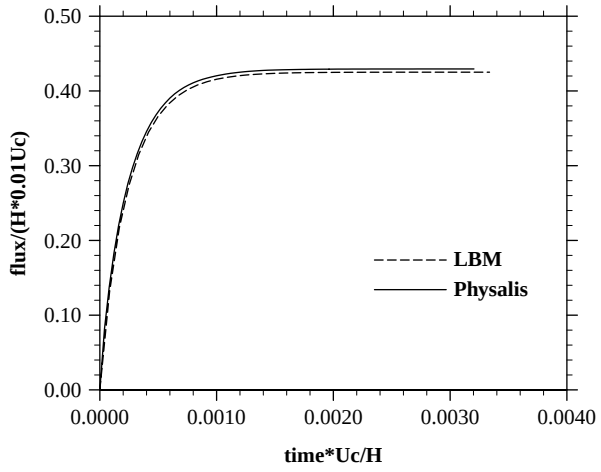

Figure 5. Comparison of results on the normalised volumetric flux as a function of time.

In Table 3, we compare forces and torques acting on each cylinder as labelled according to Figure 1. The forces are normalised by $F_0 = F_B HL$ and torques by $F_0 a$. Due to the symmetry of the geometric arrangement, only results for cylinders 1, 2, 4 and 5 are shown. For most of the cases, the relative differences between LBM and Physalis results are less than 1%. The results show that cylinder 1 experiences clockwise torque but cylinders 4 and 5 counterclockwise torques. The transverse (lift) force on cylinder 4 is the largest due to its close proximity to the wall, it also has the largest x-component force (drag) due to the combination of the flow blocking and the wall effect. We further confirm that the net force acting on fluid at the steady state, namely, the sum of reacting forces from the walls and the cylinders and the applied body force is identically zero. The normalised total tangential force acting on each wall is 0.0370 and 0.0372 for the LBM and Physalis runs, respectively.

Figures 6 and 7 display velocity distributions at three line cuts marked in Figure 1. For the streamwise velocity component, the velocity profiles are essentially identical at all three locations inside the fluid regions. It is noted that Physalis produces flows within the cylindrical particle surfaces, while in LBM no flow is computed within the cylinders. The transverse velocity also matches precisely at the AA cut where its magnitude is comparable to the streamwise component. For the other two cuts, the transverse velocity is only about one fiftieth the magnitude of the streamwise velocity. Some small differences are visible in the fluid regions, but perhaps are not important due to its very small magnitude. Note that both LBM and Physalis have roughly a second-order accuracy in spatial representation.

In the above comparisons, the actual number of time steps used in LBM is 16,000 while only 80 time steps are used in Physalis. For a given flow geometry and grid resolution, the flow Reynolds number is the only remaining governing parameter. One could therefore increase both U_c and ν proportionally in LBM to effectively reduce the number of time steps needed to produce the same macroscopic behaviour (governed by the dimensionless time tU_c/H). Taking the base case U_c value, we performed four additional runs at the same flow Reynolds number by increasing U_c by a factor of 2 (run2, $\omega = 1.333$), 4 (run3, $\omega = 1.0$), 16 (run5, $\omega = 0.40$) and 32 (run6, $\omega = 0.222$). The dimensionless flux curves are shown in Figure 8(a) for the single-relaxation time BGK collision model and in Figure 8(b) for the MRT model of Lallemand and Luo (2000). Here, ω is the relaxation frequency and is equal to $1/\tau$ in the BGK model or equal to the relaxation parameter for the stress tensor in the MRT model (Lallemand and Luo 2000). The relaxation parameters for other moments in the MRT collision model follow the suggested values in Lallemand and Luo (2000). Several interesting observations can be made. For the steady-state flow, the BGK model produces the correct result when $\omega > 1$ or there is a sufficient number of time steps (about 1000) for the flow to evolve to steady state. On the other hand, the MRT moment-space collision model can always produce the correct steady-state, even when the transient behaviour is not correct, showing an desirable advantage of MRT over BGK. During the transient time period, care must be taken to properly set the relaxation parameter in LBM, as otherwise non-physical oscillatory behaviours can occur due to the contamination of hydrodynamic modes by inherent acoustic waves in the LBM approach (Lallemand and Luo 2000, Mei *et al.* 2006).

While our current application here only concerns low Reynolds number viscous flows, our MRT LBM method can simulate a variety of flow Reynolds numbers. Figure 9

Table 3. Normalised forces and torques acting on different cylinders.

	$\tilde{F}_x$		$\tilde{F}_y$		$\tilde{\Gamma}_z$	
Particle	LBM	Physalis	LBM	Physalis	LBM	Physalis
1	0.00787	0.00781	0.0635	0.0643	−0.00286	−0.00286
2	0.0	0.0	0.0810	0.0818	0.0	0.0
4	0.0137	0.0136	0.128	0.129	0.0166	0.0166
5	0.00243	0.00241	0.0959	0.0966	0.000176	0.000188

Downloaded By: [Wang, L.-P.] At: 20:54 24 July 2008

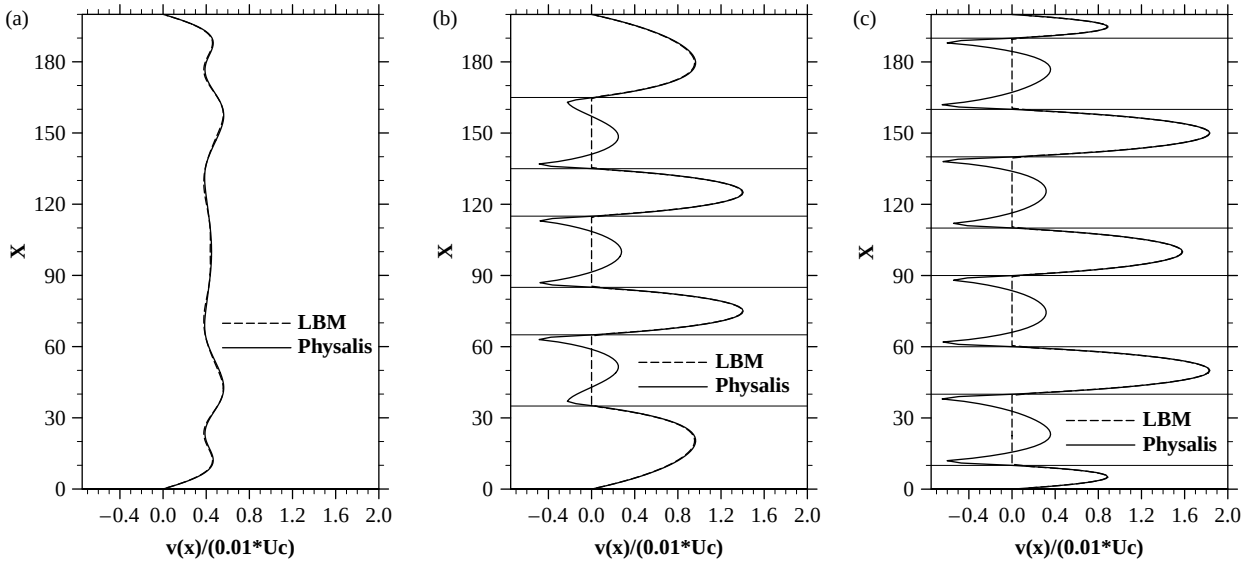

Figure 6. Comparison of steady-state, streamwise velocity profiles from LBM and Physalis at three locations shown in Figure 1. The horizontal lines mark the glass-bead boundaries when the y location cuts through glass beads. (a) AA cut; (b) BB cut and (c) CC cut.

demonstrates this capability with the same lattice resolution for a flow at a Reynolds number of about $U_s H/\nu = 1429$. Interestingly, at this Reynolds number, the long-time flow is actually unsteady due to quasi-periodic vortex sheddings and the complex interactions of vortices with cylinder surfaces and channel walls. Only half of the flow domain is shown in Figure 9. The two time snapshots in Figure 9 are both taken at the quasi-steady stage, but locally they have quite different vorticity distributions.

We now briefly discuss some preliminary results in three dimensions for a porous channel with a square cross-section, filled with 25 spherical glass beads almost packed in the channel, as illustrated in Figure 10. A moderate lattice resolution of 80 by 35 by 80 is used. Sixteen beads are located at $y = 10$, with $x, z = 10, 30, 50$ and 70. Another nine beads are located at $y = 25$, with $x, z = 20, 40$ and 60. The diameter of glass beads is set to 20. The flow is driven by a body force of magnitude equal to $8\rho\nu U_c/H^2$ where $H = 80$. The magnitude of U_c is set to give $U_c H/\nu = 288$.

Figure 11 shows the velocity distributions in two plane cuts. One can see a complex 3D flow with a large variation of local velocity magnitudes and directions, implying strong

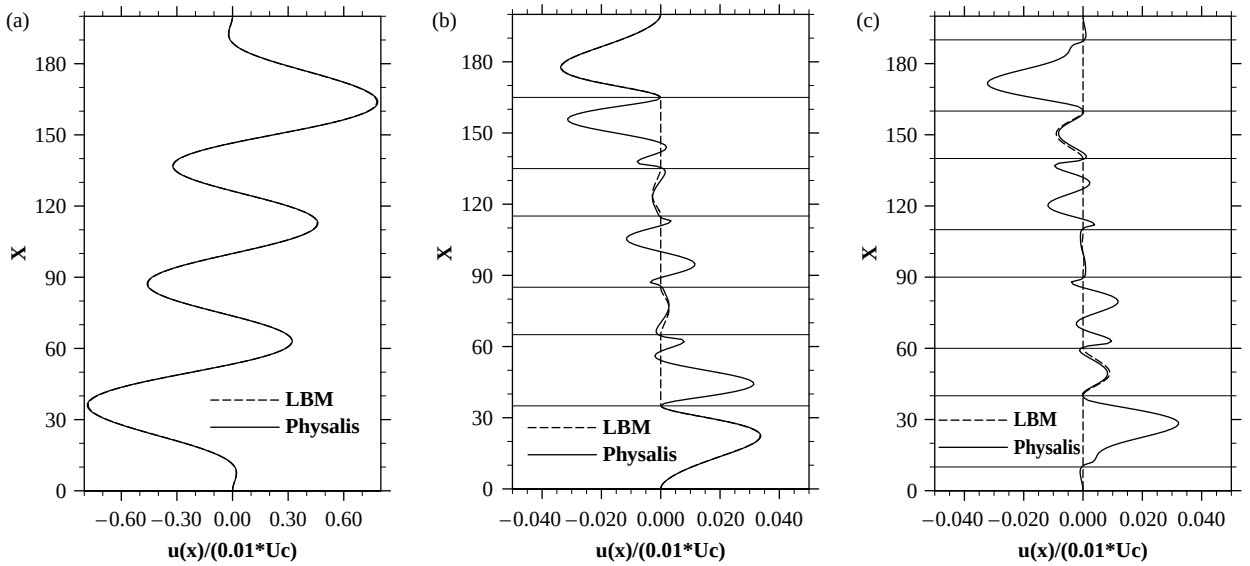

Figure 7. Comparison of steady-state, transverse velocity profiles from LBM and Physalis at the same three locations shown in Figure 1: (a) AA cut; (b) BB cut and (c) CC cut.

Downloaded By: [Wang, L.-P.] At: 20:54 24 July 2008

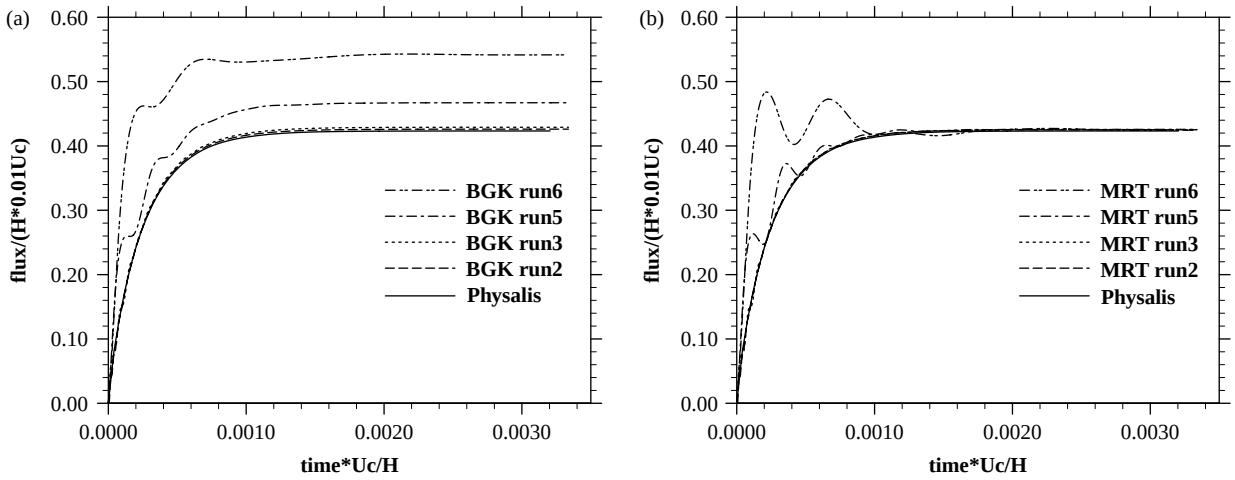

Figure 8. The normalised flux as a function of time from LBM runs at different parameter settings but the same flow Reynolds number ($U_cH/\nu = 0.2$). Run2: $\nu = 0.08333$, $U_c = 8.34 \times 10^{-5}$ and $T = 8000$; Run3: $\nu = 0.1667$, $U_c = 1.67 \times 10^{-4}$ and $T = 4000$; Run5: $\nu = 0.6667$, $U_c = 6.675 \times 10^{-4}$ and $T = 1000$; Run6: $\nu = 1.3333$, $U_c = 1.335 \times 10^{-3}$ and $T = 500$. Here, T is the total number of time steps used. (a) BGK collision model and (b) the MRT model of Lallemand and Luo (2000).

streamline curvatures in the flow. The effect of glass bead surfaces is well represented. The steady-state mean flow speed is found to be roughly $0.0005U_c$. A quantitative analysis and comparison between LBM and Physalis for this case is being undertaken and will be reported separately.

3.2 Preliminary results on colloid transport and deposition

In this section, results on the transport of colloids in the 2D porous channel with seven fixed cylinders are presented. The flow may be extended in the y-direction indefinitely using the periodicity condition to allow a colloid to travel any length in the y-direction. We used bilinear interpolation to obtain the fluid velocity at the location of a colloid. To ensure the accuracy of simulated colloid trajectories, we purposely doubled the grid resolution to 400×186 (see Table 1), although this is not necessary for the flow simulation. Figure 12 displays the locations of colloids within the same region from the inlet at a time when a total of 1898 colloids have been released into the channel, for four different mean flow speeds ranging from

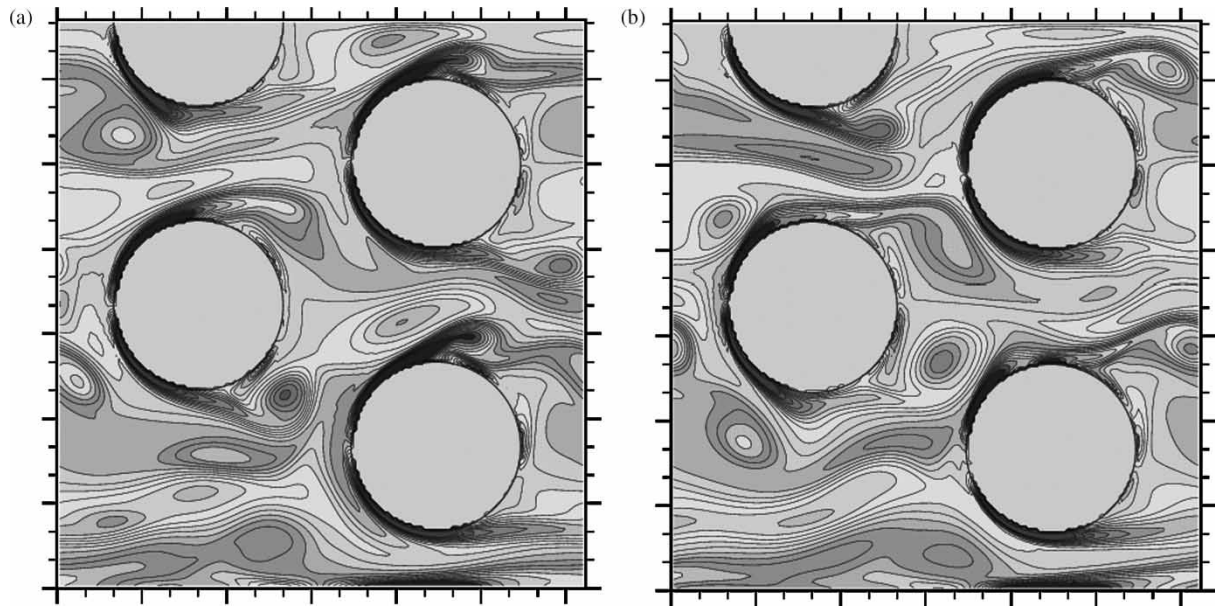

Figure 9. Two snapshots of vorticity visualisation for a test run at Reynolds number of 1429 based on the steady-state average streamwise velocity ($U_s = 0.014295$). The parameters are $U_c = 15.0$ and $\nu = 0.004$.

Downloaded By: [Wang, L.-P.] At: 20:54 24 July 2008

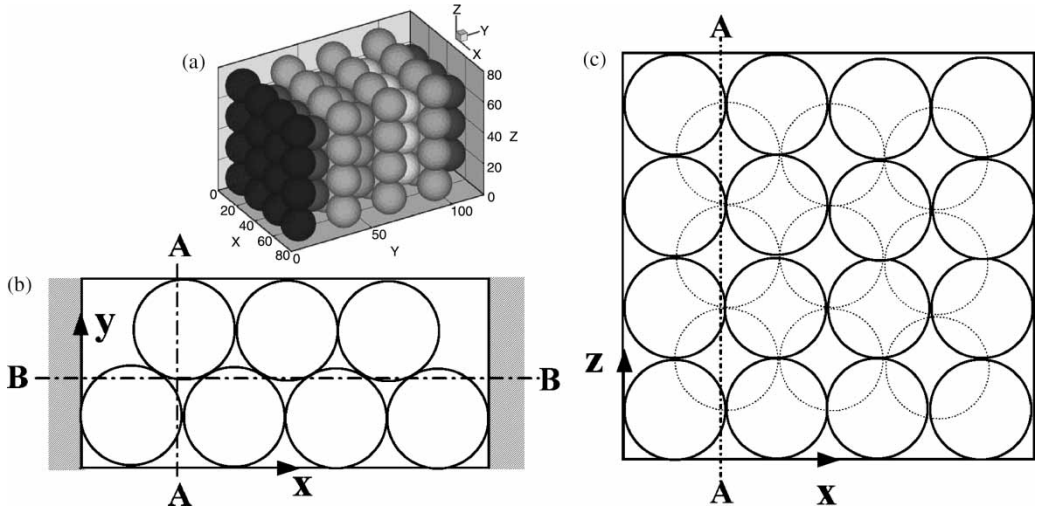

Figure 10. A 3D geometric configuration with 25 nearly packed spherical glass beads in a 3D channel with a square cross-section: (a) 3D view, (b) *xy* view and (c) *xz* view.

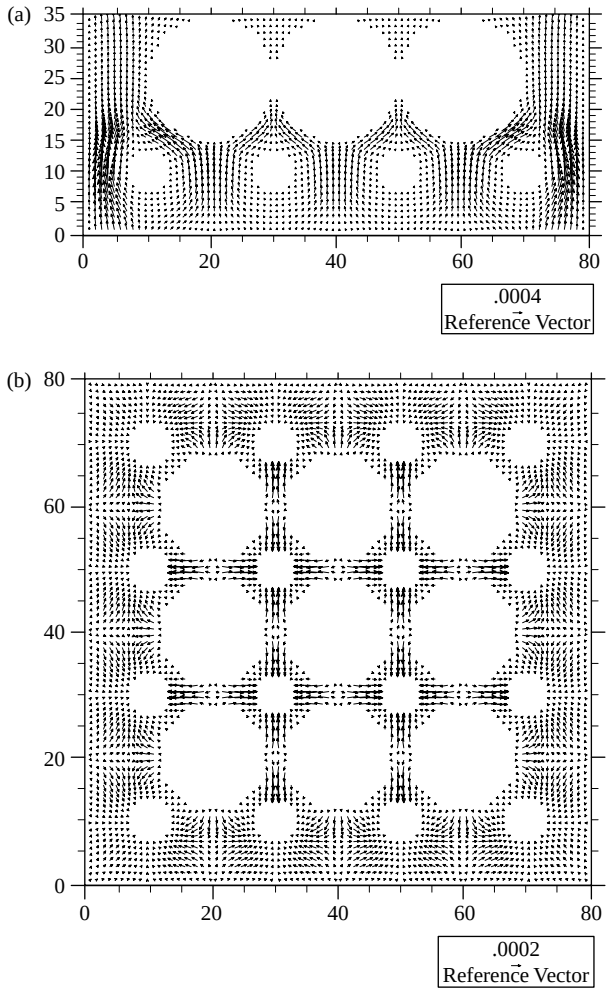

Figure 11. Simulated velocity field on two plane sections shown in Figure 10, with LBM approach. Similar results are obtained with Physalis. (a) AA plane cut and (b) BB plane cut.

1 to 8 m/day. The solution ionic strength is set to 0.1 M in these simulations. Suspended colloids are marked as open circles while deposited colloids are shown as filled circles. Since the colloid concentration is fixed at 1 ppm, a fixed total number of injected colloids corresponds to a same total solvent volume passing through the inlet. The numbers of deposited colloids at the times shown in Figure 12 are 508, 358, 231 and 105 for 1, 2, 4, 8 m/day, respectively. These results show that the overall colloidal deposition decreases with increasing flow speed.

The results were further analysed quantitatively by calculating and comparing the average surface coverage, defined as the fraction of the solid surface covered by deposited colloids. Figure 13 shows the surface coverage as a function of the total number of injected colloids. The total number $N(t)$ of injected colloids is proportional to the time t as $N(t) = \theta t(s)$, where the coefficient θ represents the number of colloids released per unit time and is 0.737, 1.474, 2.949 and 5.899 s^{-1} for the four flow speeds. The surface coverage has a quadratic dependence on the total number of injected colloids since the net rate of deposition increases roughly linearly with the injection time or the total number of injected colloids. The observed dependence on the mean flow speed may be qualitatively explained as follows. While fluid flow transports colloids along curved streamlines, Brownian motion can cause colloids to cross streamlines. The lower the mean flow speed, the longer it takes for a colloid to move through a given distance in the *y*-direction. This then increases the possibility for Brownian force to shift the colloid across streamlines and bring the colloid to regions very close to a solid surface, where the surface interaction forces can act to remove the colloid from the flow.

Downloaded By: [Wang, L.-P.] At: 20:54 24 July 2008

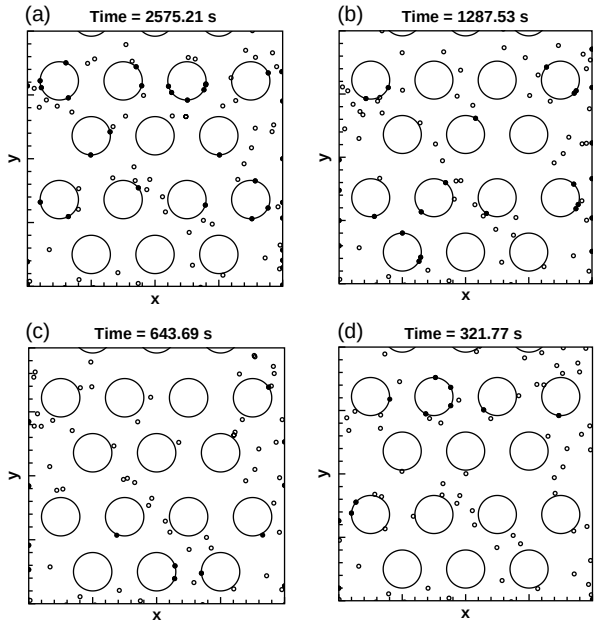

Figure 12. Colloidal distribution after injection of 1898 colloids at an interstitial velocity of (a) 1 m/day, (b) 2 m/day, (c) 4 m/day and (d) 8 m/day in 0.1 M buffer solution.

Another analysis is that we counted the number of colloids deposited on each cylinder including its periodic images. It appears that more colloids are deposited on the cylinders near the centre of the channel (Cylinders 2, 5 and 6; see Figure 1) for high flow speeds (4 and 8 m/day). But at low flow speeds (1 and 2 m/day), there is no detectable bias. This shows that the channel walls can have an effect on the deposition at high flow speeds. It should be noted that there are 170, 122, 74 and 25 colloids deposited on the channel walls for the four flow speeds, corresponding to 33.5, 34.1, 32.0 and 23.8% of total deposited colloids, respectively. This shows that the percentage of deposition on channel walls also decreases with flow speed when the flow speed is high. There are large statistical uncertainties on the data shown in Table 4, as judged by the non-symmetric distribution of the deposited colloids. Therefore, the conclusion here needs to be checked with longer simulations.

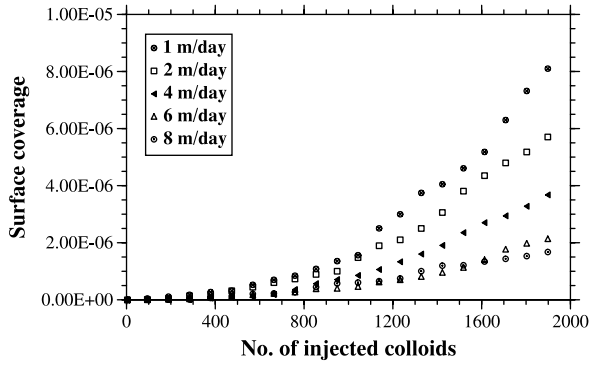

Figure 13. Predicted surface coverage of 1 μm sulphate latex colloids at different mean flow speeds with a solution ionic strength at 0.1 M.

Table 4. Number of deposited colloids on each cylinder.

Cylinder	1 m/day	2 m/day	4 m/day	8 m/day
1	46	29	14	1
2	43	31	26	5
3	38	15	18	4
4	50	52	23	14
5	48	36	20	27
6	58	39	37	22
7	55	34	19	7

Deposition on all periodic images of a cylinder are included.

We have also considered the effect of the solution ionic strength on the surface coverage and found a very non-linear dependence of surface coverage on the ionic strength (Han *et al.* 2008). A thorough analysis of surface coverage at different flow speed and solution ionic strength has been presented in our companion paper (Han *et al.* 2008), where we also show that our own experimental observations using confocal microscopy confirm the simulated dependence of colloid deposition on flow speed and ionic strength.

4. Conclusions

In this paper, we have simulated viscous flows in a model porous medium, using two different computational approaches. The fact that the mesoscopic lattice Boltzmann approach and a macroscopic CFD approach produce almost identical velocity profiles shows that both approaches are capable of handling this model geometry. Our next step will be to establish a quantitative agreement between LBM and Physalis for a realistic porous medium in three dimensions. It is believed that cross-validations of two completely different computational approaches will partially eliminate the need to perform pore-scale flow measurements.

The mesoscopic lattice Boltzmann approach is perhaps a better choice due to its simplicity in treating the no-slip boundary condition on a solid surface and its potential to extend to arbitrary flow geometry, provided that the parameters in LBM are set properly such that the results are not contaminated by acoustic waves or other numerical instabilities. The generalised LBE or MRT collision model is shown to be more robust in simulating steady-state viscous flows. Further research is needed to gain a theoretical understanding of acoustic waves in LBM for complex geometries.

A Lagrangian modelling approach for colloid transport has been developed to study the deposition of colloids on solid surface. The key finding is that the rate of deposition depends on the flow speed and solution ionic strength, and the nature of the dependence agrees qualitatively with previous observations and our visualisations using

Downloaded By: [Wang, L.-P.] At: 20:54 24 July 2008

confocal microscopy (Han *et al.* 2008). This demonstrates the feasibility of our computational model as a quantitative research tool and its potential for revealing transport mechanisms at the pore-scale. We intend to develop this model further to include other hydrodynamic interaction forces and 3D flow effects, so a quantitative comparison with pore-scale experimental observations can be made possible. It is important to note that, because typically $\kappa a_c >> 1$, the hydrodynamic interaction forces become active far before the EDL interaction force.

Acknowledgements

This study is supported by the US Department of Agriculture (NRI, 2006-02551), US National Science Foundation (ATM-0527140) and National Natural Science Foundation of China (Project No. 10628206). The authors thank Ms. V.I. Lazouskaya for helpful discussions on the general topic of colloidal transport in both saturated and unsaturated soil.

References

Aidun, C.K. and Lu, Y., 1995. Lattice Boltzmann simulation of solid particles suspended in fluid. *Journal of Statistical Physics*, 81 (1–2), 49–61.

Arcen, B., Taniere, A. and Oesterle, B., 2006. On the influence of near-wall forces in particle-laden channel flows. *International Journal of Multiphase Flow*, 32 (12), 1326–1339.

Brown, D.L., Cortez, R. and Minion, M.L., 2001. Accurate projection methods for the incompressible Navier–Stokes equations. *Journal of Computational Physics*, 168 (2), 464–499.

Chen, S. and Doolen, G.D., 1998. Lattice Boltzmann method for fluid flows. *Annual Review of Fluid Mechanics*, 30, 329–364.

Chu, Y.J., Jin, Y. and Yates, M.V., 2000. Virus transport through saturated sand columns as affected by different buffer solutions. *Journal of Environmental Quality*, 29 (4), 1103–1110.

Das, P.K. and Bhattacharjee, S., 2005. Electrostatic double layer force between a sphere and a planar substrate in the presence of previously deposited spherical particles. *Langmuir*, 21 (10), 4755–4764.

Derjaguin, B.V. and Landau, L., 1941. Theory of the stability of strongly charged lyophobic sols and of the adhesion of strongly charged particles in solutions of electrolytes. *Acta Physicochimica (USSR)*, 14, 633–662.

d'Humières, D., *et al.*, 2002. Multiple-relaxation-time lattice Boltzmann models in three dimensions. *Philosophical Transactions of the Royal Society of London A*, 360 (1792), 437–451.

Elimelech, M.J., *et al.*, 1995. *Particle deposition and aggregation: measurement, modeling, and simulation*. Oxford: Butterworth-Heinemann.

Fujita, M., *et al.*, 2004. Multiscale simulation of two-dimensional self-organization of nanoparticles in liquid film. *Japanese Journal of Applied Physics*, 43 (7A), 4434–4442.

Gao, H. and Wang, L.-P., 2007. Towards fully resolved simulation of turbulent collision of heavy particles. *CDROM proceedings of the 6th international conference on multiphase flow*, 9–13 July 2007. Leipzig, Germany.

Goldman, A.J., Cox, R.G. and Brenner, H., 1967. Slow viscous motion of a sphere parallel to a plane wall. 2. Couette flow. *Chemical Engineering Science*, 22 (4), 653–660.

Han, J., *et al.*, 2008. Pore-scale investigations of flow speed and ionic strength on colloid deposition in saturated media. *Langmuir*, Submitted.

He, X.Y. and Luo, L.-S., 1997. Lattice Boltzmann model for the incompressible Navier–Stokes equation. *Journal of Statistical Physics*, 88 (3–4), 927–944.

Hogg, R., Healy, T.W. and Fuersten, D.W., 1966. Mutual coagulation of colloidal dispersions. *Transactions Faraday Society*, 62 (522P), 1638–1651.

Inamuro, T., Maeba, K. and Ogino, F., 2000. Flow between parallel walls containing the lines of neutrally buoyant circular cylinders. *International Journal of Multiphase Flow*, 26 (12), 1981–2004.

Kim, J. and Moin, P., 1985. Application of a fractional-step method to incompressible Navier–Stokes equations. *Journal of Computational Physics*, 59 (2), 308–323.

Ladd, A.J.C., 1993. Short-time motion of colloidal particles: numerical simulation via a fluctuating lattice-Boltzmann equation. *Physical Review Letters*, 70 (9), 1339–1342.

Lallemand, P. and Luo, L.-S., 2000. Theory of the lattice Boltzmann method: dispersion, dissipation, isotropy, Galilean invariance, and stability. *Physical Review E*, 61 (6), 6546–6562.

Lallemand, P. and Luo, L.-S., 2003. Lattice Boltzmann method for moving boundaries. *Journal of Computational Physics*, 184 (2), 406–421.

Landau, L. and Lifshitz, E., 1959. *Fluid mechanics*. London: Addison-Wesley.

Maxey, M.R. and Riley, J.J., 1983. Equation of motion for a small rigid sphere in a nonuniform flow. *Physics of Fluids*, 26 (4), 883–889.

McLaughlin, J.B., 1991. Inertial migration on a small sphere in linear shear flows. *Journal of Fluid Mechanics*, 224, 261–274.

Mei, R., *et al.*, 2006. Consistent initial conditions for lattice Boltzmann simulations. *Computers and Fluids*, 35 (8–9), 855–862.

O'Neill, M.E., 1968. A sphere in contact with a plane wall in a slow linear shear flow. *Chemical Engineering Science*, 23 (11), 1293–1298.

Qian, Y.H., d'Humières, D. and Lallemand, P., 1992. Lattice BGK models for Navier–Stokes equation. *Europhysics Letters*, 17 (6BIS), 479–484.

Saffman, P.G., 1965. The lift on a small sphere in a slow shear flow. *Journal of Fluid Mechanics*, 22 (2), 385–400.

Takagi, S., *et al.*, 2003. PHYSALIS: a new method for particle simulation – Part II: two-dimensional Navier–Stokes flow around cylinders. *Journal of Computational Physics*, 187 (2), 371–390.

van Oss, C.J., 1994. *Interfacial forces in aqueous media*. New York: Marcel Dekker.

Verwey, E.J. and Overbeek, J.T.G., 1948. *Theory of stability of lyophobic colloids*. Amsterdam: Elsevier.

Yu, D., *et al.*, 2003. Viscous flow computations with the method of lattice Boltzmann equation. *Progress in Aerospace Science*, 39 (5), 329–367.

Zhang, Z. and Prosperetti, A., 2003. A method for particle simulation. *Journal of Applied Mechanics Transactions ASME*, 70 (1), 64–74.

Zhang, Z. and Prosperetti, A., 2005. A second-order method for three-dimensional particle simulation. *Journal of Computational Physics*, 210 (1), 292–324.